DOI 10.5162/sensor2017/C5.1

Finite Element Scheme for SAW Unit-Cell-Simulation

Manferd Kaltenbacher[1], Kirill Shaposhnikov[1], Pascal Nicolay[2]
[1]Institute of Mechanics and Mechatronics, Vienna University of Technolog, Austria
[2] Carinthian Tech Research (CTR AG), Villach, Austria manfred.kaltenbacher@tuwien.ac.at

Abstract:

Keywords: surface acoustic wave, finite elment formulation, periodic boundary condition

Introduction

Surface acoustic wave devices have become in use for many industrial and civil applications. Features such as passiveness, robustness, reliability, and remote-control make them attractive for telecommunications, biotechnologies, chemical industry, etc. The operating principle of piezoelectric surface acoustic wave (SAW) devices lies in the transformation of an electric input signal into an acoustic wave that propagates over the piezoelectric substrate. The surface wave is then transformed back to an electric output signal. As a rule, SAW devices operate at radio frequencies and have a tiny size. The acoustic wave is generated by a grating, which can contain up to some hundreds of electrodes. The complexity of SAW devices implies therefore their precise modelling in order to meet design and operating requirements. Here, we suggest a mathematical model for a SAW interdigital transducer based on finite element method. The model is intended to be used for computation of the parameters of SAW devices for further design and optimisation. We also concentrate on the influence of such effects as temperature and mechanical pre-stressing on the propagation of SAW. Thereby, as in the majority of models for SAW devices, we deal with the structures that have a periodic pattern and thereby turn to the model for a unit cell with periodic boundary conditions. In order to reduce computational costs, we utilise the perfectly matched layer (PML) technique to model just a small part of the substrate. The overall numerical scheme has been implemented in the finite element software CFS++ [6].

Mathematical Formulation

We consider a unit cell as displayed in Fig. 1 with a Cartesian coordinate system, where the x-axes point to the direction of wave propagation, i.e. along the grating; the y-axis is parallel to the aperture; the z-axis is orthogonal to the substrate.

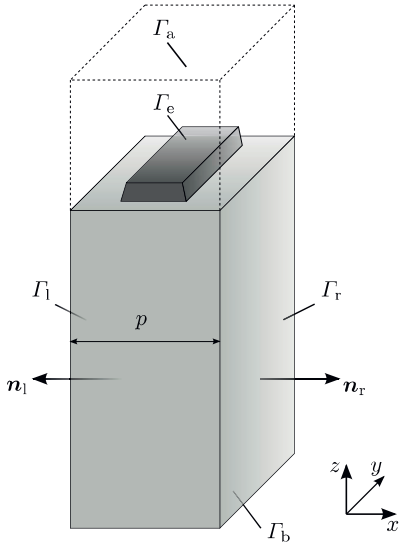

Figure 1: Principle setup of a SAW unit cell.

We presume the absence of external forces and free volume charges and a harmonic dependence on time with the angular frequency ω. Thereby, the coupled system of partial differential equations reads as

$$\mathcal{B}^T\left([\boldsymbol{c}^E]\mathcal{B}\boldsymbol{u} + [\boldsymbol{e}]^T\nabla\varphi\right) + \omega^2\rho\boldsymbol{u} = 0 \quad (1)$$

$$\nabla\cdot\left([\boldsymbol{e}]\boldsymbol{u} - [\boldsymbol{\varepsilon}^S]\nabla\varphi\right) = 0 \quad (2)$$

where $\boldsymbol{u}$ and φ act as the complex amplitudes of displacement and scalar electric potential. The material constants in (1), (2) are the tensor of mechanical moduli $[\boldsymbol{c}^E]$, the tensor of electric permittivity $[\boldsymbol{\varepsilon}^S]$, and the piezoelectric coupling tensor $[\boldsymbol{e}]$ with the first two taken at a constant electric field and a constant strain, respectively. Furthermore, $\mathcal{B}$ denotes the corresponing differential operation [6]. Within the electrodes, $\varphi = 0$, and therefore only the mechanical field is to be computed form the equation (1). On the contrary, only electric field exists in the air surrounding the device.

We impose the following boundary conditions that complement the system (1), (2):

- the structure is fixed at the bottom

$$\boldsymbol{u} = \boldsymbol{0} \text{ on } \Gamma_\mathrm{b}, \tag{3}$$

- other surfaces are free of stress

$$[\boldsymbol{\sigma}]\,\boldsymbol{n} = \boldsymbol{0} \text{ on } \Gamma_{\Omega\setminus\Omega_\mathrm{air}} \setminus \Gamma_\mathrm{b}, \tag{4}$$

- the electric field is given by a harmonic driving voltage of the amplitude V

$$\varphi = V \text{ on } \Gamma_\mathrm{e}, \tag{5}$$

- the electric potential $\varphi(\boldsymbol{x})$ vanishes in the air as $\boldsymbol{x} \to \infty$ so that, approximately,

$$\varphi = 0 \text{ on some artificial boundary } \Gamma_\mathrm{a}. \tag{6}$$

The boundary value problem (1)–(6) is still incomplete, for it lacks boundary conditions on Γ_l and Γ_r. To that end, we refer to Floquet's theorem [8]. It asserts that if $\psi(x)$ is a fundamental solution of an ordinary differential equation $f'_x(x) = A(x)\,f(x)$ with a periodic function $A(x+p) = A(x)$, then

$$\psi(x) = \psi_p(x)\,e^{xB}. \tag{7}$$

In (7), $\psi_p(x+p) = \psi_p(x)$ and $e^{pB} = \psi(p)\,\psi^{-1}(0)$. Bloch has proven that similar results are valid for the stationary Schrödinger equation with a periodic potential function (Bloch's theorem [8]) in n-dimensional space, i.e. it has a non-trivial solution of the form

$$\psi(\boldsymbol{x}) = \psi_p(\boldsymbol{x})\,e^{\mathrm{i}\boldsymbol{x}\boldsymbol{k}}, \tag{8}$$

where $\psi_p(\boldsymbol{x})$ is a periodic function. Finally, Kouchment in his work [9] extended Floquet's theory to the partial differential equations of parabolic and elliptic types. By analogy with (8), we may write

$$\boldsymbol{u}|_{\Gamma_\mathrm{r}} = \vartheta\boldsymbol{u}|_{\Gamma_\mathrm{l}} \tag{9}$$

$$\varphi|_{\Gamma_\mathrm{r}} = \vartheta\varphi|_{\Gamma_\mathrm{l}}\,; \tag{10}$$

$$[\boldsymbol{\sigma}]\,\boldsymbol{n}_\mathrm{r}|_{\Gamma_\mathrm{r}} = -\vartheta\,[\boldsymbol{\sigma}]\,\boldsymbol{n}_\mathrm{l}|_{\Gamma_\mathrm{l}} \tag{11}$$

$$\boldsymbol{D}\boldsymbol{n}_\mathrm{l}|_{\Gamma_\mathrm{r}} = -\vartheta\boldsymbol{D}\boldsymbol{n}_\mathrm{r}|_{\Gamma_\mathrm{l}}\,. \tag{12}$$

We shall refer to these equations as the Bloch-periodic boundary conditions. Now, the weak formulation of our coupled systems of PDEs may be written as

$$\int_\Omega \left(\mathcal{D}\boldsymbol{w}'\right)^T [\boldsymbol{C}]\,\mathcal{D}\boldsymbol{w}\,d\Omega - \omega^2 \int_\Omega \left(\boldsymbol{w}'\right)^T [\boldsymbol{\rho}]\,\boldsymbol{w}\,d\Omega - \int_{\Gamma_\mathrm{l}} \left(\boldsymbol{w}'\right)^T \boldsymbol{T}|_{\Gamma_\mathrm{l}}\,d\Gamma - \int_{\Gamma_\mathrm{r}} \left(\boldsymbol{w}'\right)^T \boldsymbol{T}|_{\Gamma_\mathrm{r}}\,d\Gamma = 0 \tag{13}$$

with

$$\mathcal{D}\boldsymbol{w} = \begin{pmatrix} \mathcal{B} & 0 \\ 0 & \nabla \end{pmatrix} \begin{pmatrix} \boldsymbol{u} \\ \varphi \end{pmatrix},\ [\boldsymbol{C}] = \begin{pmatrix} [\boldsymbol{c}^E] & [\boldsymbol{e}]^T \\ [\boldsymbol{e}] & -[\boldsymbol{\varepsilon}^S] \end{pmatrix}$$

$$[\boldsymbol{\rho}] = \begin{pmatrix} \rho & 0 & 0 & 0 \\ 0 & \rho & 0 & 0 \\ 0 & 0 & \rho & 0 \\ 0 & 0 & 0 & 0 \end{pmatrix},\ \boldsymbol{T} = \begin{pmatrix} [\boldsymbol{\sigma}]\,\boldsymbol{n} \\ D_n \end{pmatrix}$$

and $\boldsymbol{w}'$ being appropriate test functions. The boundary conditions (9), (12) then read

$$\boldsymbol{w}|_{\Gamma_\mathrm{r}} = \vartheta\,\boldsymbol{w}|_{\Gamma_\mathrm{l}}\,, \quad \boldsymbol{T}|_{\Gamma_\mathrm{r}} = -\vartheta\,\boldsymbol{T}|_{\Gamma_\mathrm{l}}\,. \tag{14}$$

Computational domain truncation

As mentioned in the introduction, we utilize here a perfectly matched layer to truncate the domain, which absorbs downward-propagating waves, i.e. the desired absorption in our case is performed with respect to z-coordinate.

Following the complex coordinate-stretching PML formulation [11], we replace the initial coordinate z by a stretched coordinate

$$\tilde{z} = \int_0^z s\left(\xi, \omega\right) d\xi \tag{15}$$

within the PML region Ω_{PML}, such that $d\tilde{z} \rightarrow s\left(z, \omega\right) dz$. The stretching function $s\left(z, \omega\right)$ in (15) is assumed to be complex valued within Ω_{PML}; outside it is set to $s\left(z, \omega\right) = 1$, in order to keep the coordinate unchanged ($\tilde{z} = z$).

According to the classical PML scheme, the parameter s is defined in Ω_{PML} as follows

$$s\left(z, \omega\right) = 1 + \frac{\sigma\left(z\right)}{\mathrm{i}\omega}, \ \sigma > 0, \tag{16}$$

so as to make any downward-propagating waves of the form $e^{\mathrm{i}kz}$, $k > 0$ attenuated

$$e^{\mathrm{i}kz} \rightarrow e^{\mathrm{i}kz} e^{\frac{k}{\omega}\int_0^z \sigma(\xi) d\xi}.$$

Though such a choice is useful for propagating waves, it can hardly make an evanescent wave fade away faster than it does within Ω_{PML}. For this purpose we take a different metric

$$s\left(z, \omega\right) = \kappa\left(z\right) + \frac{\sigma\left(z\right)}{\alpha\left(z\right) + \mathrm{i}\omega}, \tag{17}$$

where σ is the same as in (16), $\kappa \geq 1$, and $\alpha \geq 0$. The parameters κ and α are responsible for attenuation of evanescent and near-grazing waves, respectively [12]. The metric (17) modifies a propagating wave, such that

$$e^{\mathrm{i}kz} \rightarrow e^{\mathrm{i}k\int_0^z \kappa(\xi) d\xi} e^{\frac{k}{\omega}\int_0^z \frac{\mathrm{i}\omega\sigma(\xi)}{\alpha(\xi)+\mathrm{i}\omega} d\xi}.$$

The PML formulation utilizing the metric (17) is referred to as a complex frequency shifted PML (CFS-PML) [4]. Note, that we come up to the classical formulation setting $\kappa = 1$, $\alpha = 0$. The choice of the stretched-coordinate metrics parameters is not obvious and is usually made experimentally. This issue is, however, beyond the scope of this paper. For details, we refer to [10].

Periodic boundary condition handling

The easiest approach is to use Mortar FE formulation [6] with a Lagrange multiplier technique [7]. However, we utilize an approach based on Nitsche's idea to incooperate Dirichlet boundary conditions (see [5]) and later has been adopted by Hansbo *et al.* for non-conforming grids [1]. It can also be adopted for periodic boundary conditions [10]. In contrast to the Lagrange multipliers method, Nitsche's one does not lead to a saddle point problem. It also keeps the convergence rate of the underlying FEM model [6]. The scheme of Nitsche's method goes on as follows:

- we proceed with (13) as before but retain $\boldsymbol{T}$ on Γ_1, which yields

$$\begin{aligned} &\int_\Omega \left(\mathcal{D}\boldsymbol{w}'\right)^T \left[\boldsymbol{C}\right] \mathcal{D}\boldsymbol{w} d\Omega \\ &-\omega^2 \int_\Omega \left(\boldsymbol{w}'\right)^T \left[\boldsymbol{\rho}\right] \boldsymbol{w} d\Omega \\ &- \int_{\Gamma_1} \left(\boldsymbol{w}'\big|_{\Gamma_1} - \vartheta \boldsymbol{w}'\big|_{\Gamma_\mathrm{r}}\right)^T \boldsymbol{T}\big|_{\Gamma_1} d\Gamma = 0; \end{aligned}$$

- we add the periodic boundary condition (allowed since $\vartheta\boldsymbol{w}|_{\Gamma_1} - \boldsymbol{w}|_{\Gamma_\mathrm{r}} = 0$)

$$- \int_{\Gamma_l} \left(\boldsymbol{T}'\big|_{\Gamma_1}\right)^T \left(\vartheta\boldsymbol{w}|_{\Gamma_1} - \boldsymbol{w}|_{\Gamma_\mathrm{r}}\right) d\Gamma = 0;$$

- we add the penalisation term

$$\begin{aligned} \beta \left\|\left[\boldsymbol{C}\right]\right\| \sum_{E(\Gamma_1)} \frac{1}{h_E} \int_{\Gamma_E} &\left(\boldsymbol{w}'\big|_{\Gamma_1} - \vartheta\boldsymbol{w}'\big|_{\Gamma_\mathrm{r}}\right)^T \\ &\left(\vartheta\boldsymbol{w}|_{\Gamma_1} - \boldsymbol{w}|_{\Gamma_\mathrm{r}}\right) d\Gamma = 0. \end{aligned}$$

Here, β is a constant, $E\left(\Gamma_1\right)$ is a mesh on Γ_1, and h_E is the diameter of the element $\Gamma_E \in E\left(\Gamma_1\right)$. The vectors $T|_{\Gamma_1}$ and $T'|_{\Gamma_1}$ are defined

as follows

$$\begin{aligned}
\boldsymbol{T}|_{\Gamma_1} &= \begin{pmatrix} [\boldsymbol{\sigma}]\,\boldsymbol{n}_1|_{\Gamma_1} \\ \boldsymbol{D}\boldsymbol{n}_1|_{\Gamma_1} \end{pmatrix} \\
&= \begin{pmatrix} \left([\boldsymbol{c}^E]\mathcal{B}\boldsymbol{u} + [\boldsymbol{e}]^T\nabla\varphi\right)\boldsymbol{n}_1\big|_{\Gamma_1} \\ \left([\boldsymbol{e}]\mathcal{B}\boldsymbol{u} - [\boldsymbol{\varepsilon}^S]\nabla\varphi\right)\boldsymbol{n}_1\big|_{\Gamma_1} \end{pmatrix} \\
\boldsymbol{T'}\big|_{\Gamma_1} &= \begin{pmatrix} [\boldsymbol{\sigma'}]\,\boldsymbol{n}_1|_{\Gamma_1} \\ \boldsymbol{D'}\boldsymbol{n}_1|_{\Gamma_1} \end{pmatrix} \\
&= \begin{pmatrix} \left([\boldsymbol{c}^E]\mathcal{B}\boldsymbol{u'} + [\boldsymbol{e}]^T\nabla\varphi'\right)\boldsymbol{n}_1\big|_{\Gamma_1} \\ \left([\boldsymbol{e}]\mathcal{B}\boldsymbol{u'} - [\boldsymbol{\varepsilon}^S]\nabla\varphi'\right)\boldsymbol{n}_1\big|_{\Gamma_1} \end{pmatrix}.
\end{aligned}$$

For details, we refer to [10].

Waves in a unit cell

In a first example, we are interested in the wave solutions that propagate close to the substrate surface (i. e. pure or quasi SAW). Therefore, the waves radiating down into the substrate should be absorbed introducing a perfectly matched layer and setting

$$\boldsymbol{u} = \boldsymbol{0},\ \varphi = 0, \quad \text{on } \Gamma_0. \tag{18}$$

The remaining faces of the unit cell are stress free. We choose the 42°YX cut of $LiTaO_3$ for the substrate material. This cut, being adjusted for the wave propagation and normal directions along the x and y-axes, respectively, exhibits a leaky SAW with dominant acoustic displacements normal to the xy plane [3]. The aluminium electrode has the rectangular parallelepiped shape with dimensions $w = 0.5p$, $h = 0.1p$, and $a = 4p$. The substrate dimension in the z direction b equals $4.8p$ (see Fig. 3).

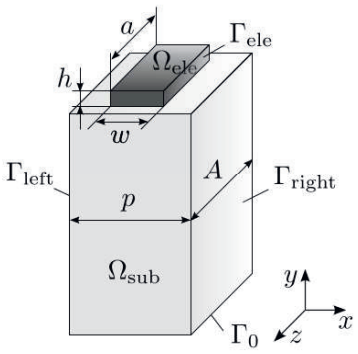

Figure 3: SAW unit cell

The results showing the distribution of the mechanical displacement and the electric potential in the unit cell at $2pf = 4000$ m/s are depicted in Figure 4. Both quantities fulfill the imposed anti-periodic boundary conditions.

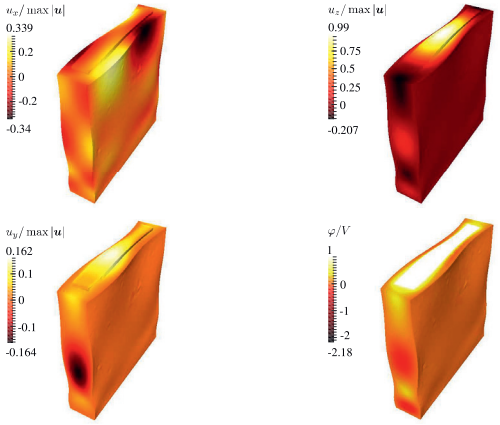

Figure 4: Mechanical displacement and electric potential in the unit cell of 42°YX-$LiTaO_3$ substrate under periodic aluminium single electrode IDT.

Lithium niobate crystal subjected to longitudinal strain

Finally, we shall investigate the strain sensitivity of a YZ-cut of a lithium niobate crystal glued to a stainless steel blade. The blade is in its turn subjected to a longitudinal deformation. The crystal can be glued to the blade in an arbitrary way such that the direction of SAW propagation and the deformation applied to the blade make up an angle α (see Fig. 5). The last can obviously lie within the range $[0°, 90°]$. The experimental analysis of this setup done at CTR AG had the goal to study how the orientation of the crystal with respect to the deformation direction affects the propagation of SAW.

DOI 10.5162/sensor2017/C5.1

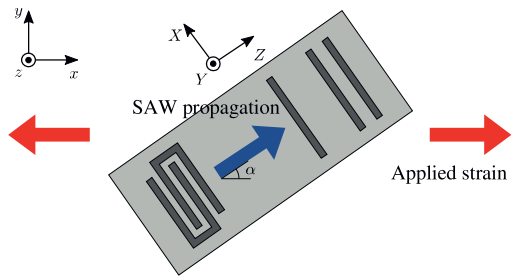

Figure 5: Position of the crystal

The results of measurements are displayed in Fig. 6 for different orientations of the crystal. It is remarkable that the slope of the sensitivity curves changes its sign from positive to negative as the angle α rises from 0° to 90°. This ensures the existence of a strain-insensible position which, according to the measurements, corresponds to the angle about 60°.

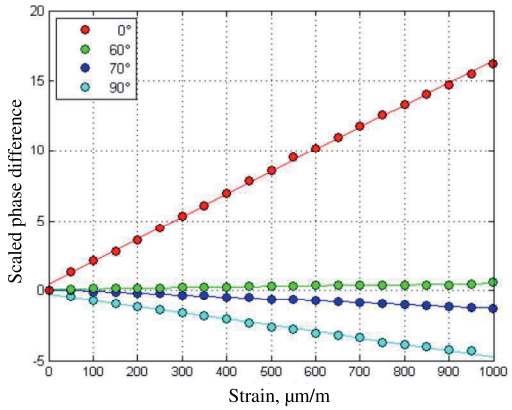

Figure 6: Results of the measurements done for different orientations of the crystal [2]

We make simulations considering the smallest (I) and the largest (II) possible values of α. First, we consider the static deformation of the structure caused by the longitudinal strain. The Cartesian coordinate systems depicted in Fig. 5 are associated with the blade (lower-case) and with the crystal principal axes (upper-case). The longitudinal strain therefore corresponds to S_x. The glue used to stick the crystal to the blade is neglected during the simulations. The stress distributions along the middle line parallel to the SAW propagation on the crystal's top are shown in Fig. 7 (a) and (b) for cases I and II respectively. For the second step we use the extracted values of the stress neglecting the edge effects. Namely, the stress distribution is taken uniform over the whole crystal with the same value as that at the centre point of the crystal's top surface.

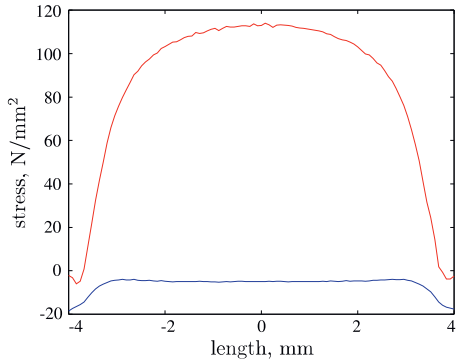

(a) Case I

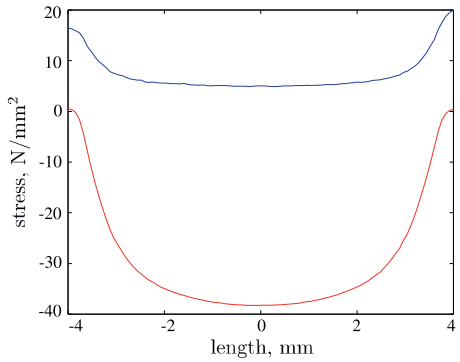

(b) Case II

Figure 7: Stress distributions on the crystal's top along the SAW propagation direction: σ_Z (red) and σ_X (blue)

The relative velocities for the setups I and II are

$$\left.\frac{\Delta v}{v}\right|_{\mathrm{I}} = -1.7533 \cdot 10^{-4}$$
$$\left.\frac{\Delta v}{v}\right|_{\mathrm{II}} = 5.8444 \cdot 10^{-5}.$$

The relative phase shift between the incident and the reflected signal is calculated and

equals

$$\delta\psi_{\mathrm{I}} = \left.\frac{\Delta\psi}{\psi}\right|_{\mathrm{I}} = 7.7904 \cdot 10^{-4},$$
$$\delta\psi_{\mathrm{II}} = \left.\frac{\Delta\psi}{\psi}\right|_{\mathrm{II}} = -2.6164 \cdot 10^{-4}.$$

Then we can find the ratio between the phase shifts in cases I and II:

$$\frac{\delta\psi_{\mathrm{II}}}{\delta\psi_{\mathrm{I}}} \approx -0.336.$$

According to Fig. 6, the ratio between the slopes of the red and the cyan curves, which correspond to setups I and II, is approximately equal to -0.3. This shows that the results obtained from the measurements and the simulations are in a good agreement with one another considering the assumptions we have made during the modelling.

References

[1] A. Hansbo, P. Hansbo, and M. G. Larson. A finite element method on composite grids based on Nitsche's method. *ESAIM: Math. Model. Numer. Anal.*, 37:495–514, 2003.

[2] B. Maier. *Design of a test procedure and characterization of the correlation between strain and SAW propagation time in single crystals.* Master thesis, FH-Kärnten, 2011.

[3] D. Morgan. *Surface acoustic wave filters with applications to electronic communications and signal processing.* Elsevier Ltd., 2nd edition, 2007.

[4] F. H. Drossaert and A. Giannopoulos. A nonsplit complex frequency-shifted PML based on recursive integration for FDTD modeling of elastic waves. *Geophysics*, 72(2):T9–T17, 2007.

[5] J. Nitsche. Über ein Variationsprinzip zur Lösung von Dirichlet-Problemen bei Verwendung von Teilräumen, die keinen Randbedingungen unterworfen sind. *Abh. Math. Sem. Univ. Hamburg*, 36(1):9–15, 1971.

[6] M. Kaltenbacher. *Numerical Simulation of Mechatronic Sensors and Actuators: Finite Elements for Computational Multiphysics.* Springer, 3 edition, 2015.

[7] M. Aubertin, T. Hennerson, F. Piriou, P. Guerin, and J.-C. Mipo. Periodic and anti-periodic boundary conditions with the lagrange multipliers in FEM. *IEEE Trans. Magn.*, 40(8):3417–3420, 2010.

[8] M. S. P. Eastham. *The spectral theory of periodic differential equations.* Scottish Academic Press, Edinburgh, 1973.

[9] P. A. Kouchment. Floquet theory for partial differential equations. *Russ. Math. Surv.*, 37(1):1–60, 1982.

[10] K. Shaposhnikov. *Finite Element Simulation of Piezoelectric Surface Acoustic Wave Sensors.* PhD thesis, Vienna University of Technology, Austria, 2016.

[11] W. C. Chew and W. H. Weedon. A 3d perfectly matched medium from modified Maxwell's equations with stretched coordinates. *Microwave Optical Tech. Letters*, 7(13):599–604, 1994.

[12] Y. F. Li and O. Bou Matar. Convolutional perfectly matched layer for elastic second-order wave equation. *J. Acoust. Soc. Amer.*, 127(3):1318–1326, 2010.